Evaluation of H-/D- Density Using Langmuir Probe Measurement in a Cs Seeded Negative Ion Source

Evaluation of H-/D- Density Using Langmuir Probe Measurement in a Cs Seeded Negative Ion Source

Evaluation of H-/D- Density Using Langmuir Probe Measurement in a Cs Seeded Negative Ion Source

E. Rattanawongnara[2], M. Osakabe[1,2], H. Nakano[1,3], K. Tsumori[1,2], K. Nagaoka[1,3], and Y. Takeiri[1]
[1]National Institute of Fusion Science (NIFS), [2]SOKENDAI University, [3]Nagoya University
(e-mail: engrhyt.rattanawongnara@nifs.ac.jp)

Abstract. An electron reduction model is reintroduced for Langmuir probe plasma density profile measurement. The model is compared with conventional laser photo-detachment measurements and can predict negative ion density in the 2-3 x $10^{17}m^{-3}$ range using correlation factors for hydrogen and deuterium cases. The calibration and correction procedure is demonstrated for application to ion sources.

1. Introduction

Neutral Beam (NB) Injection is a strong candidate for the current drive and heating scheme in future tokamak-based fusion reactors such as ITER and JA-DEMO [1,2,3]. The current drive by NB injection is robust and can be applied at the density range of reactor-relevant plasmas if its injection energy is sufficiently high. Considering the conversion efficiency from charged particle beam to NB at the high energy of 1MeV [4,5], which is the required injection energy of NB at ITER, the negative-ion beam technology is necessary. Although several negative-ion-based NB injectors have already been developed and operated [6,7,8] and extensive studies of negative ion sources have been done [9], negative ion production and its extraction mechanisms still need to be fully understood. Thus, it is necessary to investigate the negative-ion behavior near a beam extraction hole to understand the mechanisms and improve the performance of negative-ion-based NBI [10].

The conventional techniques for measurement of negative ion density, such as Photo-Detachment-assisted Langmuir Probe (PDLP) and Cavity Ring-Down (CRD) measurements, rely on the Photo-Detachment (PD) process and the injection of the laser pulse is necessary to invoke the process. Injecting the laser pulse near the PG hole is difficult because the grid-supporting structure scrapes off the pulse before reaching the extraction hole. For this reason, we developed a new method to evaluate negative-ion density using a conventional Langmuir probe measurement [11].

In this paper, we apply our method to deuterium plasmas for the first time. Section 2 shows the experimental setup and calibration between PDLP and CD. Section 3 shows the evaluation of negative ion density from the Langmuir Probe (LP) with an electron reduction model. In section 4, the results from LP and PDLP are compared and discussed. Section 5 is the conclusion of the paper.

2. Experimental Setup

The negative ion source, Research and Development Negative Ion Source at the National Institute for Fusion Science (NIFS-RNIS) [12], shown in Fig. 1(a), is our primary device for this study. This filament arc-type ion source operates with a hot filament to produce arc discharge. We control

negative ion density changing arc power, which varies between 30 to 70kW for these experiments. The discharge is operated with 0.3Pa for Hydrogen and Deuterium, achieving the same negative-ion density range displayed on the CRD result. The ion source is equipped with cusp magnets to improve electron confinement in the discharge region and a filter magnet (FM) to reduce the temperature of electrons in the beam extraction region. The magnetic field produced by the FM separates the extraction and discharge regions [13]. The Electron Deflection Magnets (EDM) are installed in the extraction grid (EG) to reduce co-extracted electrons in the beam [14,15]. The magnetic field strength of all magnets is shown in Fig. 1(b), which will be used for discussion in a later section. The extraction region starts from the filter field to the area inside the PG aperture. This region is our focus for the Langmuir probe experiment. Cesium vapor is introduced from the back plate of the ion source to enhance negative-ion production on the PG surface [16,17]. The PG is biased with a 1.6V power supply between the PG and the discharge chamber [18]. CRD and PD diagnostic are installed on the ion source to measure negative ion density.

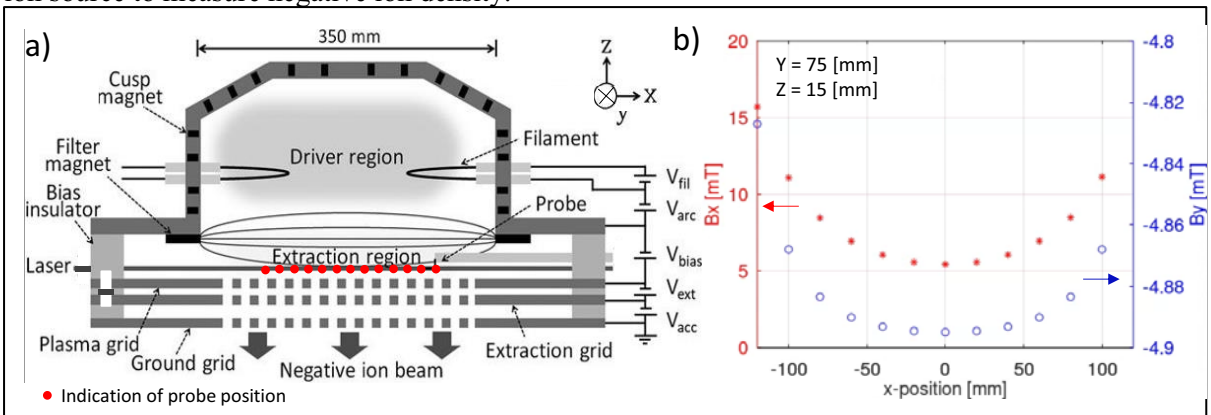

Fig. 1(a) shows a schematic drawing of NIFS-RNIS discharge chamber in horizontal cross-section and (b) magnetic field strength in x and y direction at each probe position.

CRD diagnostic consists of a YAG laser to generate a laser beam pulse, a cavity with 99.98% reflectivity mirrors to perform multiple reflections to enhance the sensitivity of the measurement and a photodetector. The photodetector is placed behind the cavity mirror at the opposite end of the laser injection side in order to detect the decay time of the laser intensity [19,20]. The negative ion photo-detachment process absorbs the laser traveling between the cavity mirrors. The line integrated negative ion density can be calculated from the decay time using the Lamber-Beer law, as shown in eq. 1 [21].

$$n(H^-, D^-) = \frac{d}{c\sigma L}\left(\frac{1}{\tau} - \frac{1}{\tau_0}\right) \text{ , --- (1)}$$

where L is the length of the plasma region in the cavity, σ is the absorption cross-section, and d is the cavity length. The τ and τ_0 is the decay time of laser intensity with and without plasma, respectively.

Langmuir probe measurements in this experiment combine PDLP and conventional LP. The two operations are time synchronized with a specific voltage sweep waveform. The waveform started with a constant probe voltage at 40Volt for PDLP, where a laser pulse is triggered during this phase and the increment of electron currents associated with the laser injection is observed [22,23]. After the laser injection, the probe voltage starts to sweep down for the conventional LP operation, and the cycle repeats. The probe is installed on a linear drive with a movable bellow to move the probe position on the horizontal axis of the ion source. Using movable bellows instead of a Wilson seal reduces the risk of air leaks during the scanning. This change drastically improves the cesium condition in the experiment shown in this paper compared to the previous experiment [24].

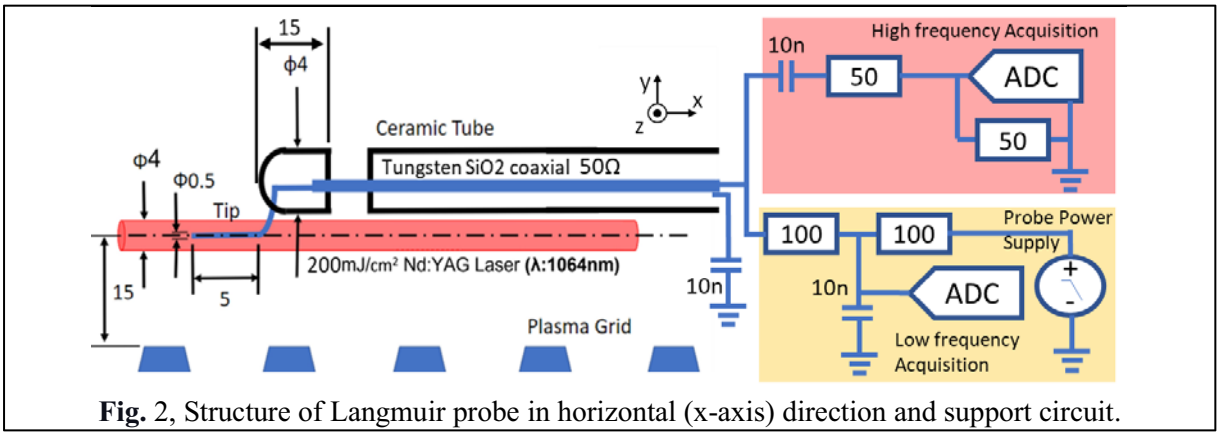

Fig. 2, Structure of Langmuir probe in horizontal (x-axis) direction and support circuit.

As shown in Fig. 2, the LP structure consists of a probe tip made of tungsten wire with 0.5mm in diameter and 5mm in length. The probe wire is covered in ceramic to prevent heat from plasma. The 1064nm YAG laser beam we use in this experiment is divided for CRD and PDLP. The beam is attenuated to achieve 200mJ/cm2 laser flux for PDLP. The diameter of the laser column is set to 4mm with 0.3 degrees divergent, and the path length from the final focusing lens to the middle of the ion source is 500mm. The center of the laser beam is aligned with the center of the probe tip. The alignment is checked with laser printing from 5 different probe positions. Figure 2 also shows the circuit used in this experiment. The circuit branches into a low-frequency branch for probe voltage scan and probe current detection in LP operation, while the high-frequency branch blocks DC voltage from passing and is connected to a 500MHz acquisition system (NI PXIe-5160) for measuring the increment of electron current in PDLP operation. The PDLP data in the current unit will be calibrated for negative ion density with CRD, which is an integral line measurement. The PDLP spatial profile is integrated with the trapezoidal integral, which provides a calibration factor shown in eq. 2 [24,25].

$$k_{pd} \int_{x1}^{x2} \Delta I_e(x, Parc)dx = \left(\int_0^L n_-(x)\,dx\right)_{CRD(Parc\_average)} \quad \text{---(2),}$$

where k_{pd} is the calibration factor for PDLP current, ΔI_e is the PDLP current data point, n_- is the negative ion density, and x is the center position of the probe tip. Figure 3(a) shows that the probe measurement range is insufficient to detect the end of the plasma span. This scanning length left the calculation with an integral limit problem. In this case, we decided to use ion source dimension x1 = -175mm and x2 = 175mm, shown in Fig. 1 (a) as an integral limit, and the integral profile is shown in Fig. 3(a). Figure 3(b) shows a linear correlation between the integral of the PD profile and the line integral CRD negative ion density. The slope of the linear fitting gives the calibration factor used for estimating point density from PD, as shown in eq. 3.

$$n_-(x) = k_{pd}\,\Delta I_e(x) \quad \text{---(3)}$$

The correlation factors of Deuterium and Hydrogen are comparable values. The cause of the discrepancy between PD and CRD mainly came from estimating the integral limit. Another cause of discrepancy can be assumed as interference from laser ablation [26] or current overshoot from plasma sheath oscillation as electrons abruptly appear in the laser column.

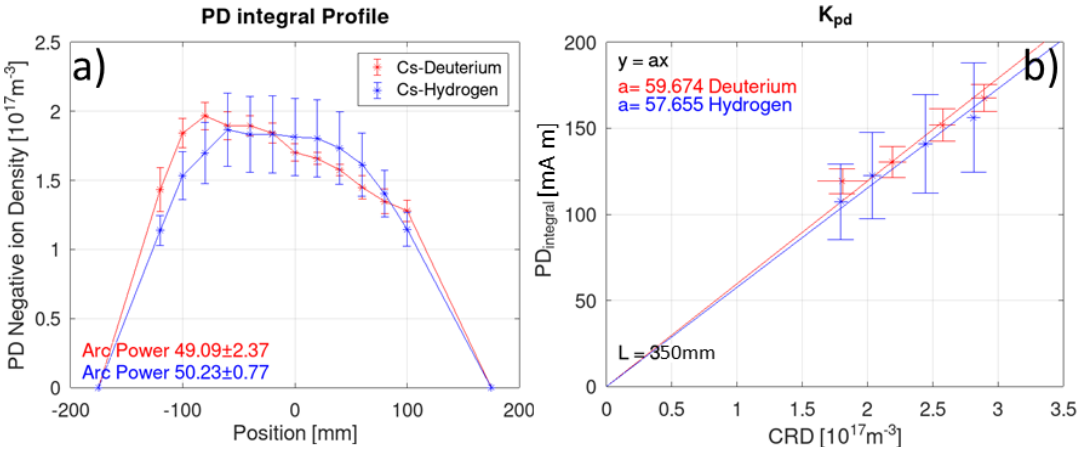

Fig. 3 shows (a) PD integration profile where integral limit is estimated at position -175 and 175mm and (b) linear correlation between integral value of the PD profile and line integral density from CRD.

3. Analysis

The electron reduction method [11] is reintroduced in this paper to perform negative ion evaluation of Deuterium and Hydrogen plasma in NIFS-RNIS. The eq. 4 explain the method,

$$n_- = \frac{\sqrt{\frac{dI_+^2}{dV}} - \beta\sqrt{\frac{dI_-^2}{dV}}}{\frac{qA_i}{2\pi}\sqrt{\frac{8q}{\pi m_i}}(1-\beta)} \quad \text{---- (4)}$$

Where A_i is a probe geometry area, q is a charge value, dI_+^2/dV is a slope from negative saturation current-square, dI_-^2/dV is a slope from positive saturation current-square. The β, by definition, is a ratio of square root of mass different between ion and electron where, m_i is an ion mass, and m_e is an electron mass and different between probe absorption area of electron and ion where A_e is a probe electron absorption area, and A_i is a probe geometry area [11]. Empirically, when considering electron-positive ion plasma, we can derive β from the Orbital Motion Limit theory (OML), which is defined by a ratio of the square root of negative saturation current-square and positive saturation current-square as written in eq. 5.

$$\beta \equiv \frac{A_e}{A_i}\sqrt{\frac{m_i}{m_e}} = \sqrt{\frac{dI_+^2}{dI_-^2}} \quad \text{---(5)}$$

The β ratio is measured in a non-cesiated plasma for electron-positive ion condition, where an electron and positive ion maintain charge neutrality according to the definition in eq.5.

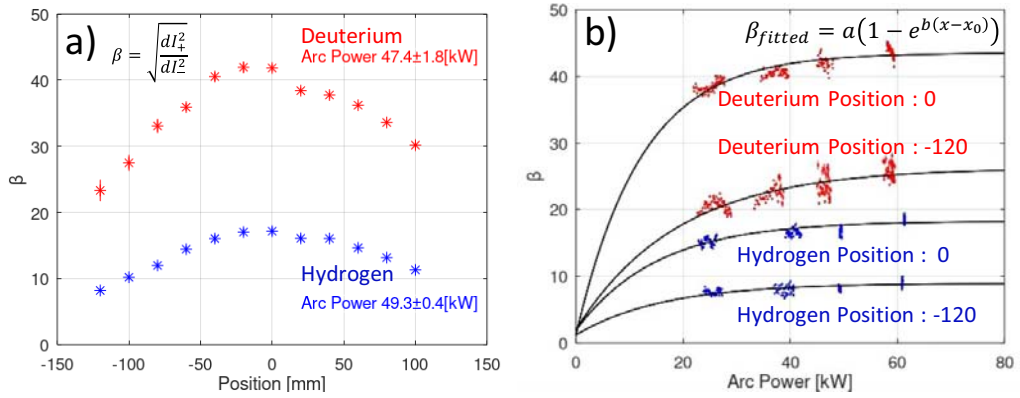

Fig. 4 the β ratio is measured at 12 points between -14 to 10 cm from the center, where red is measured from the Deuterium case, blue is the Hydrogen case, (a) is a profile of measured β ratio in the ion source, and (b) β ratio versus arc power at the center point of probe scanning profile.

Figure 3(a) shows the β ratio empirically found to be primarily changed by the magnetic field, which correlate to the magnetic field profile in Fig. 1(b). From the fig. 3(a), our β ratio shows the value from 8 to 18 for Hydrogen and 22 to 42 for the Deuterium case. The magnetic field dependence of β is confirmed by the theoretical point of view that the effective area for the probe to absorb electrons is reduced under the applied magnetic field. At the same time, the ion is considered inert to the magnetic field effect [27]. The size of the probe absorption area for electrons mainly depends on magnetic field strength and the thermal velocity of the electrons due to the size of the electron Larmore radius [27]. However, the unknown parameters, such as sheath radius, may contribute to the change in the absorption area. For this reason, the β ratio may also depend on many plasma parameters. Fortunately, the β ratio versus Arc power is saturated in our measurement range, as shown in Fig. 4(b). The arc power control in our ion source primarily controls all plasma parameters, such as plasma density and temperature. Therefore, the saturate tendency of β versus the arc power indicates that β mainly depends on the ion's mass and magnetic field strength. Although the saturation is obtained, we use the saturation function (see [11]) to estimate the β value for the correction of electron thermal velocity.

Another aspect of the β ratio is about the effective ion mass. In general, ion sources produce multiple species of positive ions, H+, H2+, and H3+, which introduces the need for an effective ion mass ratio [28]. The arc power change may lead to a change in the effective ion mass ratio, which is empirically included in the β ratio. However, besides the effective mass included in the β ratio, using H+ mass in eq. 4 causes ambiguity and will contribute to diverting the correlation factor from unity. Fortunately, the correlation factor is intended to be used for correcting the negative ion measurement of PDLP; therefore, the issue of the effective ion mass can be automatically solved, but only for negative ion density.

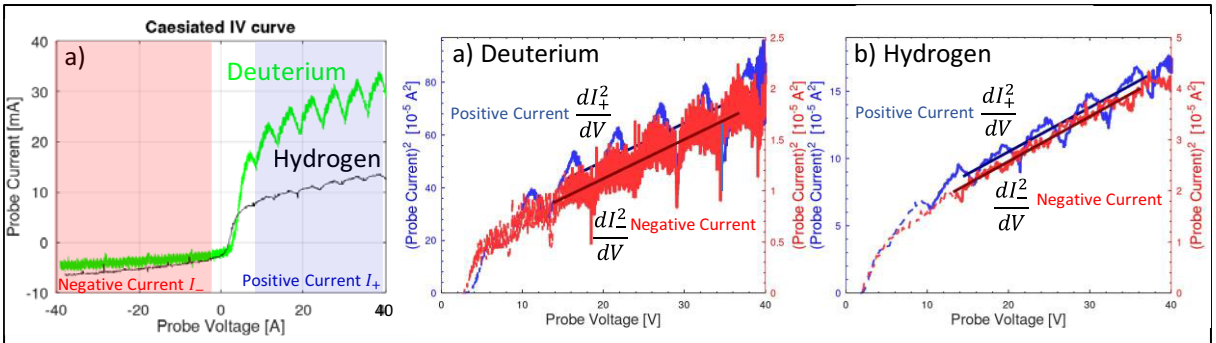

Fig. 5 shows analysis of I-V curve from LP where (a) shows *I-V* curve from caesiated Deuterium (green) and Hydrogen (black) plasma, (b) and (c) shows $I^2 - V$ curve analysis for Deuterium and Hydrogen plasma, respectively.

$I - V$ curves from caesiated and non-caesiated plasma are analyzed in the same manner as shown in Fig. 5. As seen in Fig. 5(a), the caesiated *I-V* curve from Deuterium shows a larger positive current than the Hydrogen case, which indicates a more electron concentration in the plasma. Fig. 5(b) and (c) show the Deuterium and Hydrogen plasma analysis, respectively. The analysis begins with calculating for $I^2 - V$ and finding a dI_+^2/dV slope in the voltage range from 15 to 35 volts and a dI_-^2/dV slope from -35 to -15 volts. The voltage range is called a saturation region which allow the approximation of OML where $V > V_s$ and $I = \frac{qnA}{4}\sqrt{\frac{kT}{2\pi m}\left(1 + \frac{q(V-V_s)}{kT}\right)}$ can approximated into $I \cong \frac{qnA}{4}\sqrt{\frac{q(V-V_s)}{2\pi m}}$ for the assumption to be applied. The slope from the analysis will apply to eq. 4 for negative-ion density evaluation. The ripple in the *I-V* curve and $I^2 - V$ curve is an AC ripple from the ion source arc power supply. The linear least square fitting is used for this analysis's fitting problems. Because ripple is a periodic signal, the effect is self-cancel and gives a 2% error in the general result.

4. Result and Discussion

The analyzed results from PD and LP with the electron reduction method are compared to verify the possible use of the electron reduction method. Firstly, the negative-ion density profile of LP measurements is plotted, as shown in Fig. 6(a).

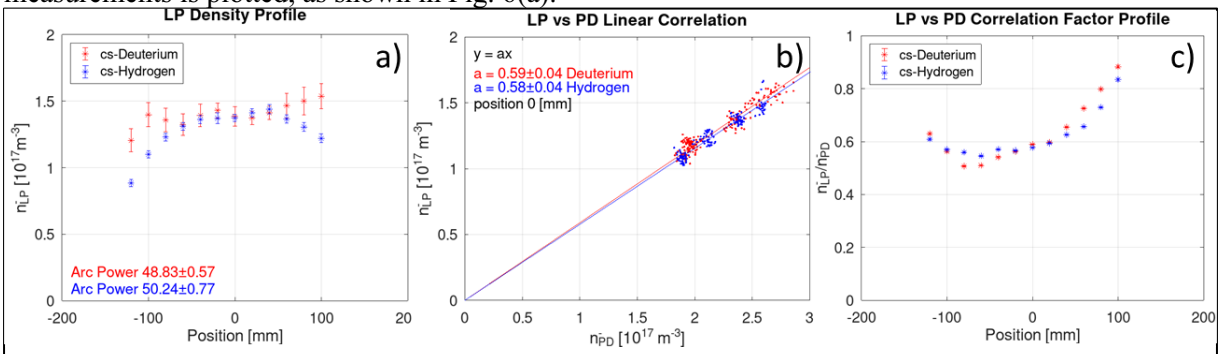

Fig. 6 shows (a) negative ion density from LP, (b) linear correlation between LP and PD, and (c) profile of correlation factor.

Figure 6(b) shows a linear correlation between negative ion density from LP and PD at probe position 0mm (center of the ion source). At the probe position 0mm, the negative ion density is between 1.7 and 2.8x$10^{17}m^{-3}$ for Hydrogen and Deuterium. Positive ion Density is between 1.4 and 2.5 x $10^{17}m^{-3}$ for Hydrogen and between 1.1 and 1.7 x $10^{17}m^{-3}$ for Deuterium. We also observed the electronegativity (n^-/n_e) change from 7.5 to 15 in Hydrogen and 1.8 to 4.8 in Deuterium. The data for correlation fitting are taken from arc power 30 to 70kW. The linear correlation function is utilized because the two measurements are in the negative-ion domain. The correlation appears linear enough within the data point span, and the correlation factor is 0.59 from Deuterium and 0.58 from Hydrogen. The correlation factor's value may show the edge-to-center effect of the LP [29,30]. Because PD is calibrated with CRD, the negative ion density is reliable. In contrast, an electrostatic probe is invasive and suffers from plasma sheath influence. Figure 6(c) shows the correlation factor profile with position dependence, which can be used for density correction. The magnetic field from FM may be responsible for the position dependence of the correlation factor profile. The negative-ion density result between LP and PD shows linear correlation, and the correlation factor profile from Deuterium and Hydrogen shows similarity, confirming that the method can be applied for negative-ion evaluation in this density range.

Further development of the model for a more precise density profile is needed as we now understand that the magnetic field primarily affects the prediction of negative-ions density. We may consider theoretical correction for electron absorption area as shown in ref. 27.

5. Conclusion

The electron reduction method is verified in this research to be a candidate for negative ion density evaluation with LP in the density range 2-3 x$10^{17}m^{-3}$. The profile of negative ions from LP with the electron reduction method have factor of two discrepancy with calibrated PD when correction factor is not used. However, the technique allows the use of simple LP as a benefit with a 10% error when correct with a correlation factor.

References

[1] R. S. Hemsworth et al., New J. Phys. **19**, 025005 (2017).
[2] U. Fantz et al., Fusion Engineering and Design **159**, 111760 (2020)
[3] K. Tobita et al., Fusion Science and Technology **75**:5, 372-383 (2019)
[4] K. H. Berkner et al., *Plasma neutralizers for H− or D− beams*, the production and neutralization of negative hydrogen ions and beams, *2nd Int. Symp.*, Upton, NY, USA176 (1980).
[5] C. Hopf et al., Nucl. Fusion **61**, 106032 (2021)
[6] Y. Takeiri et al., FST **58,** 482 (2009)

[7] M. Osakabe et al., NF **62,** 042019 (2022)
[8] M. Kuriyama et al., FED **115,** 39-40 (1998)
[9] V. Dudnikov, Development, and application of negative ion source, Springer 110 (2019)
[10] N. D. Harder et al., JINST **18**, C08005 (2022)
[11] E. Rattanawongnara et al., Plasma and Fusion Research **18**, 1401020 (2023)
[12] S. Masaki et al., *Rev. Sci. Instrum*. **91** (2020) 013512
[13] D. Wünderlich et al., J. Appl. Phys. **130**, 053303 (2021)
[14] S. Geng et al., JSPF **10**, 3405016 (2015)
[15] G. Chitarin et al., Rev. Sci. Instrum. **85**, 02B317 (2014)
[16] K. Nagaoka et al., AIP conf. **1390,** 374 (2011)
[17] K. Tsumori et al., Rev. Sci. Instrum. **83**, 02B116 (2012)
[18] H. Nakano et al., AIP Conf. Proc.s **1515**, 237 (2013)
[19] H. Nakano et al., AIP conf. **1390**, 359 (2011)
[20] H. Nakano et al., JINST **11**, C03018 (2016)
[21] G. Berden and R. Engeln, John Wiley and Sons Ltd. (2009)
[22] M. Bacal, Rev. Sci. Instrum. **71**, 3981–4006 (2000)
[23] L. Friedland et al., Phys. Rev. E **49**, 5 (1994)
[24] S. Masaki et al., Rev. Sci. Instrum. **91**, 013512 (2020)
[25] S. Geng et al., AIP Conf. Proc. **1655**, 040014 (2015)
[26] R. Dodd et al., Plasma Sources Sci. Technol. **19**, 015021 (2010)
[27] M. Usoltceva et al., Phys. of Plasm. 25, 063518 (2018)
[28] L. Schiesko et al., AIP Conf. Proc. 2052, 040006 (2018)
[29] P. Chabert and N. Braithwaite, Radio-Frequency Plasmas, Cambridge University Press, Cambridge (2011)
[30] J-L Raimbault and P Chabert, Plasma Sources Sci. Technol. **18**, 014017 (2009)